RSC Advances

PAPER

Cite this: *RSC Adv.*, 2023, **13**, 20844

Removal of hydrogen sulfide in the gas phase by carbide slag modified bentonite

Qi Jiang,[a] Ming Jiang, *[a] Tianci Han,[b] Yongmei He,[a] Tianguo Li,[a] Jilai Zhang,[a] Youbo Su,[a] Yonglin Wu,[a] Bo Dian[a] and Yonglan Zong[a]

Bentonite-based adsorbents for the removal of hydrogen sulfide (H_2S) were prepared by a wet-mixing method using carbide slag as the active component. The effects of carbide slag content, calcination temperature, calcination time, and reaction temperature on the H_2S adsorption capacity were investigated. The results showed that compared with the blank bentonite adsorbent, the carbide slag-modified bentonite-based adsorbent enhanced the chemisorption of H_2S. The adsorption capacity of the carbide slag modified bentonite adsorbent (2.50 mg g^{-1}) was more than 40 times higher than that of the blank bentonite-based adsorbent (0.06 mg g^{-1}) under optimal conditions. The optimal conditions for H_2S removal were 3 : 5 ratio of carbide slag-to-bentonite, calcination temperature of 450 °C for 2 h, and reaction temperature of 95 °C. H_2S was mainly removed in the mesopores and macropores of the adsorbent and was finally transformed to CaS and sulfate on the adsorbent surface. The adsorption process of H_2S followed the Freundlich adsorption isotherm equation and Bangham adsorption kinetic model.

Received 21st May 2023
Accepted 4th July 2023

DOI: 10.1039/d3ra03392a

rsc.li/rsc-advances

1. Introduction

Hydrogen sulfide (H_2S) is a highly toxic compound with an irritating odor that is produced during natural gas production, the processing of coal and its derivatives, oil refining, sewage treatment plants, and landfills.[1] H_2S can seriously corrode equipment and pipelines and must be treated before being discharged into the environment.[2,3] Currently, the industrial removal of H_2S is primarily performed by wet removal methods, but the green removal of H_2S is difficult.[4–6] Dry desulfurization methods are simple, stable, and produce little secondary pollution.[7–9] Adsorption is the most commonly used dry desulfurization method, but during the H_2S adsorption, the loss of adsorbent is large, which decreases the desulfurization effect and increases the cost of its removal and purification.

Bentonite is a non-metallic mineral with montmorillonite as its main mineral component. It is one of the most abundant clay minerals in the world and has been used because of its good water absorption, swelling properties, and non-toxicity.[10–12] Bentonite is also used in environmentally friendly materials. Stepova *et al.*[13] used metal-modified carbonate-rich bentonite for the purification of H_2S in low concentration exhaust gases. The results showed that the iron-modified and copper-modified bentonite adsorbents had almost 100% H_2S removal capacity by 15 min and 25 min, respectively. Similar results were obtained by Nguyen-Thanh *et al.* who used metal-modified bentonite compounded with activated carbon for H_2S purification.[14] The results showed that 3000 ppm H_2S could be almost completely removed by the copper-modified adsorbent by 10 min. Currently, bentonite-based adsorbents for H_2S removal are usually modified using iron chloride solution or copper chloride solution.[13,14] However, the formation of Fe_2S_3 and CuS is a challenge for the effective utilization of such type adsorbents. The utilization of solid waste can ensure green development goals are achieved, and waste-to-waste technologies have emerged as a new idea for the comprehensive utilization of waste. Bentonite-based adsorbents can be modified with waste material and used for H_2S removal.

Carbide slag is a highly alkaline and relatively loose surface solid waste residue produced by the hydrolysis of calcium carbide to produce acetylene for PVC production. Its main component is $Ca(OH)_2$.[15] The global annual production of carbide slag is huge, each 1 ton of PVC produces about 1.5–2 tons of carbide slag by-product, and the massive dumping of carbide slag poses a serious threat to the environment.[16] Therefore, scholars have utilized the high alkalinity of carbide slag to prepare materials to remove SO_2, HCl, fixed CO_2.[16,17] However, composites containing carbide slag have not been used for H_2S removal.

In this paper, a carbide slag-modified bentonite adsorbent for H_2S removal was prepared. The effects of carbide slag content, calcination temperature, calcination time, and adsorption temperature on the adsorptive removal of H_2S were

[a]*College of Resources and Environment, Yunnan Agricultural University, Kunming, China. E-mail: mingjiang2010@163.com*
[b]*Shandong Pengrun New Materials Co. Ltd., Jining, China*

investigated by H_2S removal efficiency curves. The adsorption characteristics of H_2S on the adsorbent were analyzed by SEM, N_2-BET, FTIR spectroscopy, Raman spectroscopy, XRD, and XPS. The H_2S adsorption isotherms and kinetic were also explored.

2. Experimental

2.1. Materials

2.1.1. Bentonite and carbide slag. Sodium-based bentonite (noted as B) with a fineness of 45 μm was purchased from Lingshou Dehang Mineral Products Co., Ltd., China.

Activated bentonite (noted as AB) was obtained by the high-temperature calcination of sodium-based bentonite at 450 °C for 2 h.

Carbide slag (noted as CS) was collected from a calcium carbide plant in An Ning, Yunnan Province, China.

2.1.2. Preparation of bentonite-based adsorbents. Adsorbents were prepared from sodium-based bentonite, activated bentonite, and carbide slag by wet mixing and calcination activation (Fig. 1). The adsorbents abbreviations and synthesis conditions as shown in Table 1.

Activated bentonite does not bond well with calcium carbide slag; therefore, a total of 10 adsorbents were prepared, which were noted as CK-B, CK-AB, C-B, C-AB, CS-B (1 : 5), CS-B (2 : 5), CS-B (3 : 5), C-CS-B (1 : 5), C-CS-B (2 : 5), and C-CS-B (3 : 5). The maximum loading of carbide slag on bentonite under the experimental conditions was 3 : 5, beyond which the adsorbent could not be bonded into shape.

Fig. 1 shows the preparation process of the adsorbents. Volatile impurities were removed from carbide slag by calcination. The diameter specification of the extrusion machine and ball rolling board was 3 mm; therefore, the diameter of the prepared spherical adsorbents was 3 mm. During aging, the raw material needs to be evenly infiltrated by water to prevent the disintegration of the adsorbent due to water vaporization during calcination. The aging time was generally 24 h.

2.2. Analysis and characterization methods

Scanning electron microscopy (SEM) images were obtained on Nova NanoSEM field emission scanning electron microscope (Frequency Electronics, Inc., USA). Chromium was used as a conductive material to coat the samples.

N_2-BET isotherms were measured with a Quadrasorb Evo fully-automatic specific surface and pore size distribution analyzer (Quantachrome, Inc., USA).

Raman spectra were collected with a LabRAM HR Evolution Raman spectrometer (Horiba, Inc., Japan). The wavenumber range was 50–4000 cm^{-1}.

X-ray diffraction (XRD) measurements were performed using an X'Pert3 powder X-ray diffractometer (PANalytical, Inc., Netherlands).

X-ray photoelectron spectroscopy (XPS) was carried out using a K-Alpha X-ray photoelectron spectrometer (Horiba, Inc.,

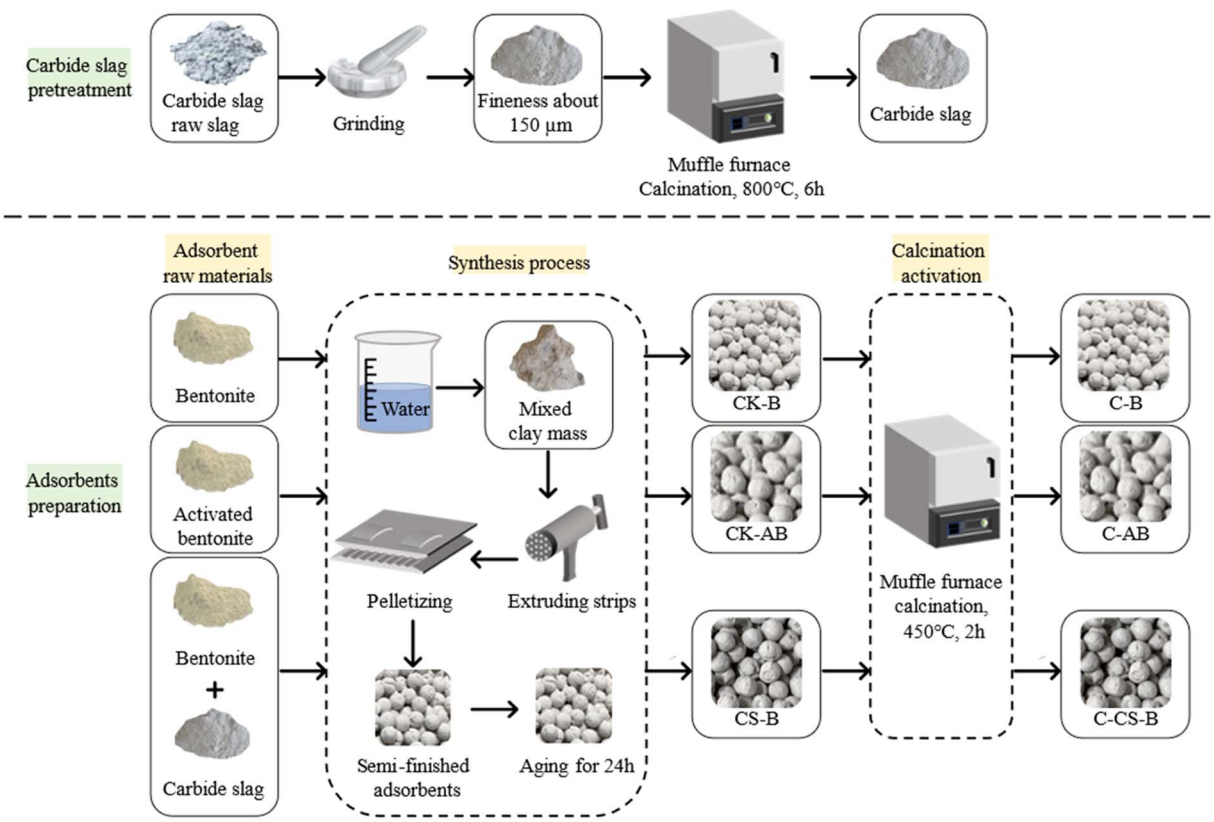

Fig. 1 The preparation process of adsorbents.

Table 1 The adsorbents abbreviations and synthesis conditions

Name of adsorbent	Mass ratio of raw materials	Calcination temperature	Calcination time
CK-B	Bentonite : Water = 5 : 2, wt/wt	—	—
C-B	Bentonite : Water = 5 : 2, wt/wt	450 °C	2 h
CK-AB	Activated bentonite : Water = 3 : 2, wt/wt	—	—
C-AB	Activated bentonite : Water = 3 : 2, wt/wt	450 °C	2 h
CS-B (1 : 5)	Carbide slag : Bentonite : Water = 1 : 5 : 3.5, wt/wt/wt	—	—
C-CS-B (1 : 5)	Carbide slag : Bentonite : Water = 1 : 5 : 3.5, wt/wt/wt	450 °C	2 h
CS-B (2 : 5)	Carbide slag : Bentonite : Water = 2 : 5 : 4.5, wt/wt/wt	—	—
C-CS-B (2 : 5)	Carbide slag : Bentonite : Water = 2 : 5 : 4.5, wt/wt/wt	450 °C	2 h
CS-B (3 : 5)	Carbide slag : Bentonite : Water = 3 : 5 : 5, wt/wt/wt	—	—
C-CS-B (3 : 5)	Carbide slag : Bentonite : Water = 3 : 5 : 5, wt/wt/wt	450 °C	2 h

Japan). The excitation source was Al Kα rays ($h\nu$ = 1486.6 eV) with a beam spot of 400 μm.

FTIR spectra were collected using a Nicolet iS10 FTIR spectrometer (Thermo Fisher, Inc., USA). The wavenumber range was 4000–400 cm^{-1}.

TD-DTG was collected with HCT-1 synchronous TG-DTA thermal analyzer (Beijing Hengjiu Experimental Equipment Co. Ltd., China).

2.3. H_2S breakthrough capacity

A dynamic H_2S adsorption device was designed under laboratory conditions to evaluate the ability of the adsorbent to remove H_2S, in Fig. 2. A mixture of H_2S and N_2 was flowed into the gas buffer tank and obtained the desired H_2S concentration (850 mg m^{-3}). The total gas flow rate was adjusted to 100 mL min^{-1}. U-shaped glass tubes (inner diameter 17 mm) were used to fix the adsorbent. The pre-sorption H_2S concentration was labeled as C_0 and the post-sorption H_2S concentration was labeled as C. The mass of the adsorbent was 5 g. The concentration of H_2S was measured using a gas chromatograph (GC9790II, Zhe Jiang Fuli Analytical Instruments Co., Ltd., China). The test was stopped after the penetration point concentration, which was defined as 10% of the pre-adsorbed H_2S concentration ($C/C_0 = 0.1$).[18] After the test, the adsorption capacity of H_2S was calculated with the following integral formula:[19]

$$q = \left(QC_0t - Q\int_0^t C\mathrm{d}t \right) \Big/ m \quad (1)$$

In this formula, q is the adsorption capacity (mg g^{-1}); Q is the total gas flow (m^3 min^{-1}); t is the adsorption time (min); C_0 is the pre-sorption H_2S concentration (mg m^{-3}); C is the post-sorption H_2S concentration (mg m^{-3}); m is the adsorbent quality (g).

3. Results and discussion

3.1. Adsorption of H_2S by different types of bentonite-based adsorbents

The hydrogen sulfide breakthrough capacity curves for the prepared bentonite adsorbents are presented in Fig. 3. Only the adsorbents modified by carbide slag with high-temperature activation showed a higher H_2S adsorption capacity. Except for C-CS-B (1 : 5), other adsorbents rapidly penetrated and deactivated at the start of the test.

According to the H_2S breakthrough curves, the breakthrough adsorption capacities of CK-B, C-B, CK-AB, C-AB, CS-B (1 : 5), and C-CS-B (1 : 5) were 0.06, 0.06, 0.06, 0.05, 0.05, and 0.23 mg g^{-1}, respectively. Comparing these adsorbents shows that high-temperature calcination negatively affected the single bentonite adsorbent, while the bentonite adsorbent loaded with carbide slag was suitable for high-temperature

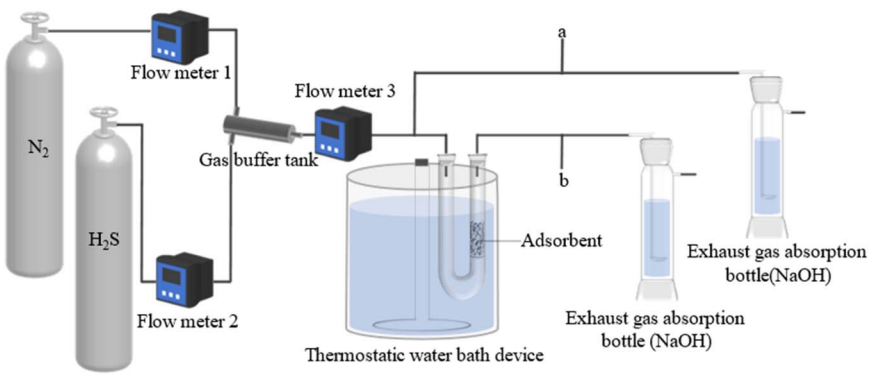

Fig. 2 Dynamic H_2S adsorption device.

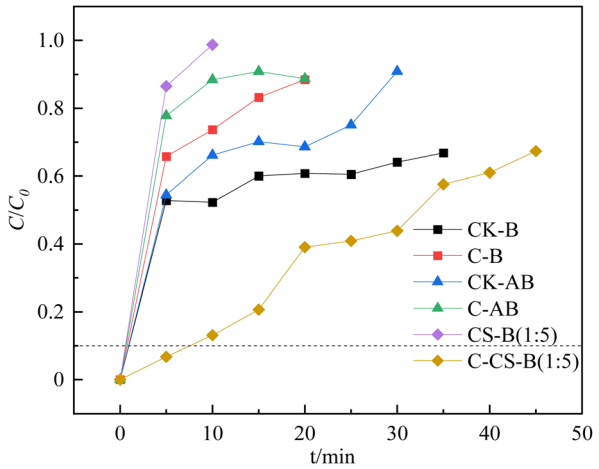

Fig. 3 Breakthrough curves of H_2S on different bentonite-based adsorbents at 20 °C.

activation. The excellent adsorption performance of C-CS-B (1 : 5) may be due to the active groups formed after the introduction of $Ca(OH)_2$.

3.2. Evaluation of the performance of H_2S removal

The effects of the carbide slag content on CS-B adsorbents for H_2S adsorption removal are shown in Fig. 4(a). According to the adsorption experiments, the carbide slag content was important for removing H_2S. Fig. 4(a) shows that the H_2S removal efficiency was enhanced upon increasing the carbide slag content. When the ratio of carbide slag to bentonite was 3 : 5, the H_2S penetration time of C-CS-B (3 : 5) was extended to about 55 min. And the presence of H_2S is barely detectable until 30 minutes. In the study by Stepova *et al.*[13] using Fe-modified bentonite and Cu-modified bentonite for H_2S removal, the time of appearance of H_2S at the outlet was about 17 min and 25 min, respectively. Therefore, carbide slag modified bentonite seems to have more potential for H_2S removal. In addition, the breakthrough adsorption capacity increased from an initial value of 0.06 mg g^{-1} (CK-B) to 0.92 mg g^{-1}. Therefore, the carbide slag content directly affected the adsorption activity. Properly increasing the carbide slag content in the adsorbent increased the coverage of the active sites on the bentonite and accelerated the desulfurization reaction.

As mentioned in Fig. 1, the calcination temperature of the carbide slag-modified bentonite adsorbent (CS-B) was 450 °C. This temperature was chosen based on the TG-DTA curve of

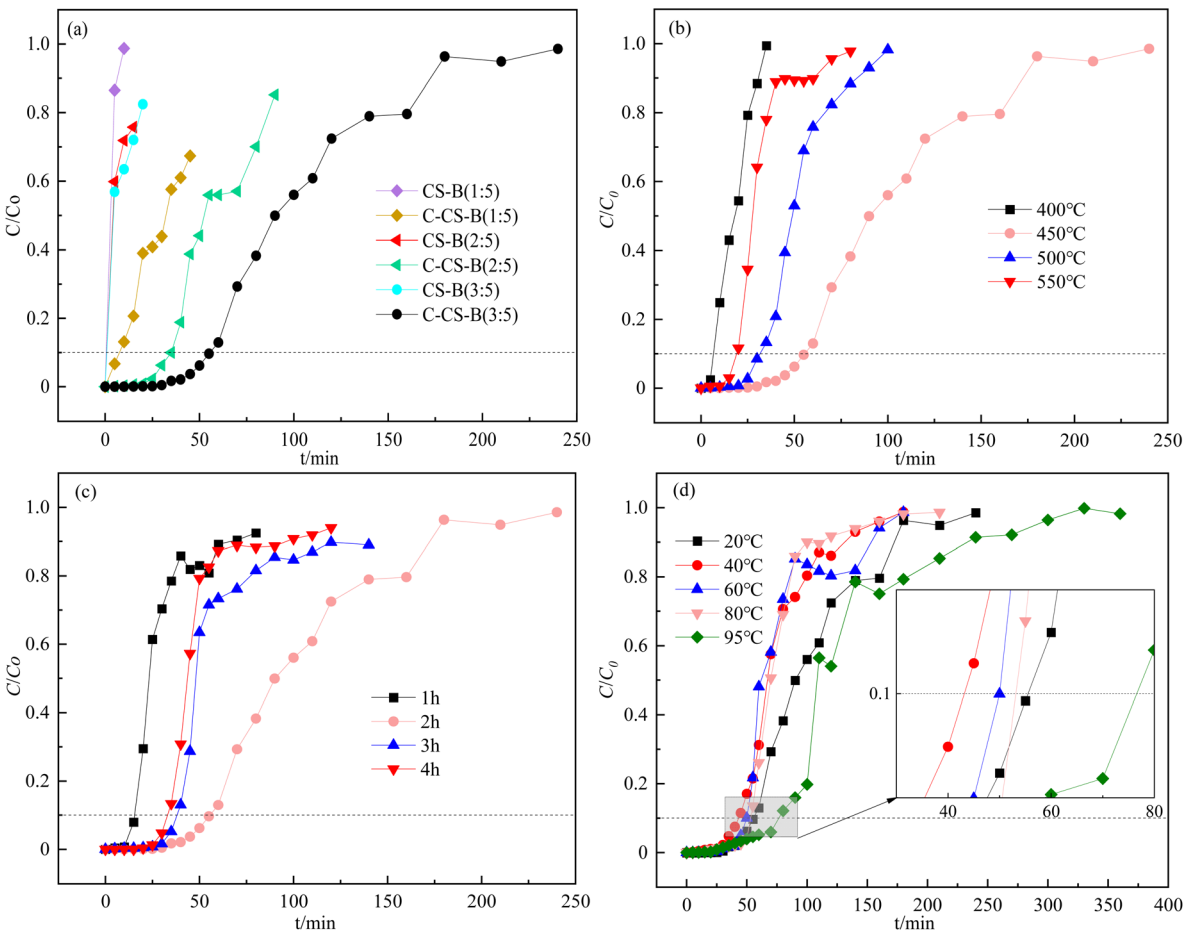

Fig. 4 (a) Breakthrough curves of H_2S using different carbide slag contents at 20 °C. (b) Influence of calcination temperature on the breakthrough curves of H_2S. The calcination time was set to 2 h. (c) Influence of calcination time on the breakthrough curves of H_2S. The calcination temperature was set to 450 °C. (d) Influence of adsorption temperature on the adsorption performance of H_2S.

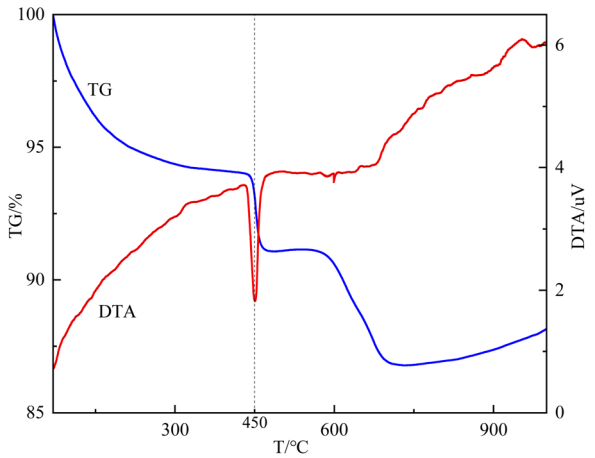

Fig. 5 TG-DTA curves of CS-B (3 : 5).

the sample CS-B, as shown in Fig. 5. The TG curve showed an obvious weight loss plateau in the range of 430–475 °C, corresponding to heat absorption decomposition peak in the DTA curve. This indicated that phase transformations occurred in the CS-B (3 : 5) adsorbent at 430–475 °C, which changed its adsorption performance. To accurately determine the optimum temperature and time for adsorbent activation, a single-factor experiment was conducted to examine the effect of the calcination temperature and time. Both the calcination temperature and calcination time greatly influenced the H_2S adsorption capacity. In agreement with the results in TG-DTA curves, 450 °C was the optimal calcination temperature (Fig. 4(b)). Fig. 4(c) confirms that 2 h was the optimal calcination time. When the calcination was low or the calcination time was too short, no reaction between carbide slag and bentonite was observed. The surface physicochemical properties of the adsorbent were insufficient to support the adsorption of large amounts of H_2S. A high calcination temperature or long calcination time might sinter the adsorbent, which will reduce the adsorption performance of H_2S

The adsorption reaction temperature is one of the most important factors affecting the adsorption of H_2S by adsorbents. According to Fig. 4(d), upon increasing the adsorption temperature, the H_2S adsorption capacity decreased and then increased. As observed, when the adsorption temperature increased from 20 °C to 40 °C, the penetration time decreased from about 55 min to 45 min. And when the adsorption temperature continued to increase, the breakthrough time increased until the maximum value was reached at 95 °C, at which time the breakthrough time was about 75 min and the adsorption capacity was about 2.50 mg g^{-1}. Therefore, the adsorption process of H_2S on C-CS-B (3 : 5) was divided into

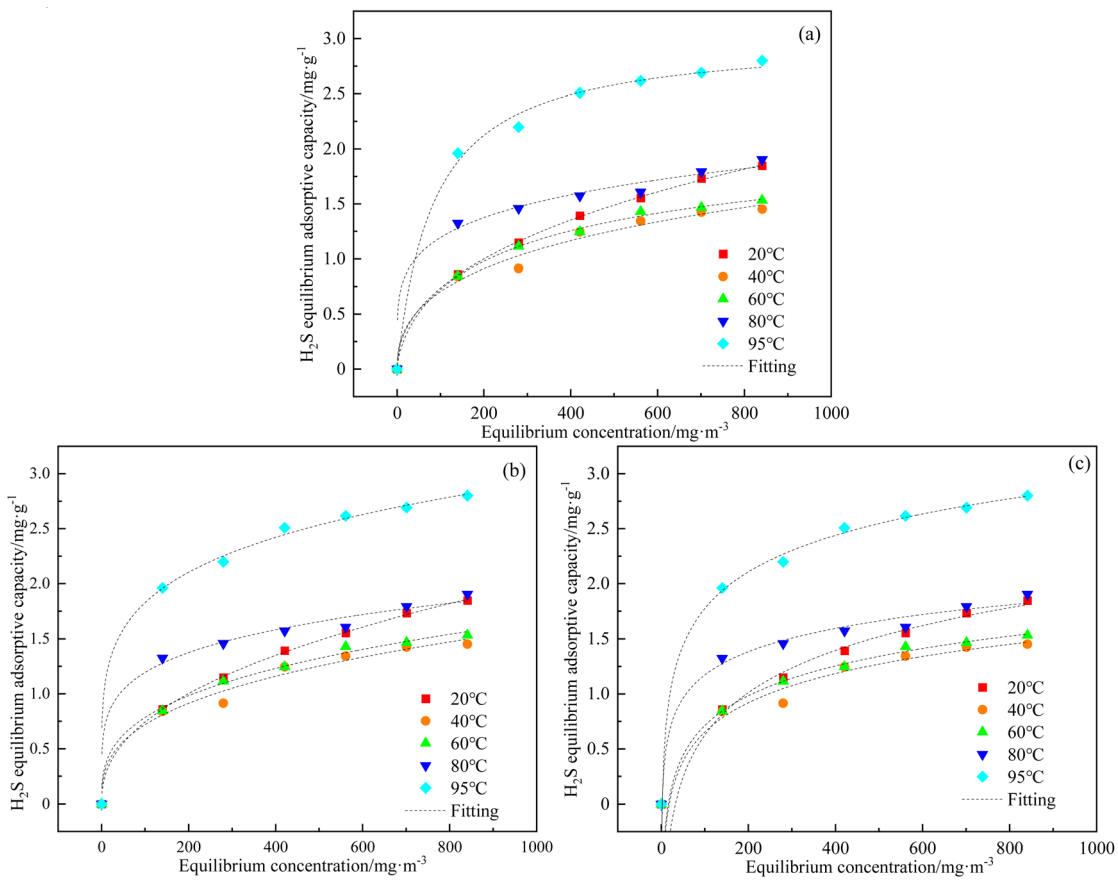

Fig. 6 (a) Langmuir; (b) Freundlich; (c) Temkin adsorption isotherm fits for H_2S adsorption over C-CS-B (3 : 5).

Table 2 Langmuir, Freundlich, and Temkin model parameters for adsorption of H_2S on C-CS-B (3 : 5)

		Temperature				
Isotherm model	Parameters	20 °C	40 °C	60 °C	80 °C	95 °C
Langmuir	q_m	17.21922	5.23121	2.24395	55.00686	3.01403
	b	0.00520	0.02022	0.01899	0.00849	0.01191
	R^2	0.99865	0.89846	0.98692	0.88666	0.94171
Freundlich	$q_m k$	0.10266	0.14741	0.17595	0.46926	0.71740
	n	0.42999	0.34425	0.32466	0.20288	0.20299
	R^2	0.99888	0.92294	0.97946	0.91581	0.98049
Temkin	a_0	0.03086	0.05482	0.06188	0.46446	0.40331
	f	1.80063	2.60573	2.55853	3.27514	2.08390
	R^2	0.98464	0.91262	0.98957	0.88633	0.98043

two stages, which indicated that the mechanism of H_2S adsorption on C-CS-B (3 : 5) adsorbent may be a physical and chemical adsorption process. This phenomenon might be caused that in the low temperature stage (20–40 °C), the physical adsorption process was inhibited as the temperature increased and showed a tendency to decrease the adsorption performance. While the reaction temperature exceeds 40 °C, the adsorption process was dominated by endothermic chemical reaction process, which showed the best adsorption performance at 95 °C. In particular, the adsorption capacity of C-CS-B (3 : 5) was more than 40 times higher than that of CK-B (0.06 mg g^{-1}) at the optimal conditions of 95 °C. In the study by Nguyen-Thanh *et al.*[14] the $CuCl_2$ modification of activated carbons with bentonite resulted in a 5 times higher H_2S breakthrough capacity of the modified adsorbent than the blank adsorbent. In this way, the modification of bentonite with carbide slag may provide better performance in H_2S removal.

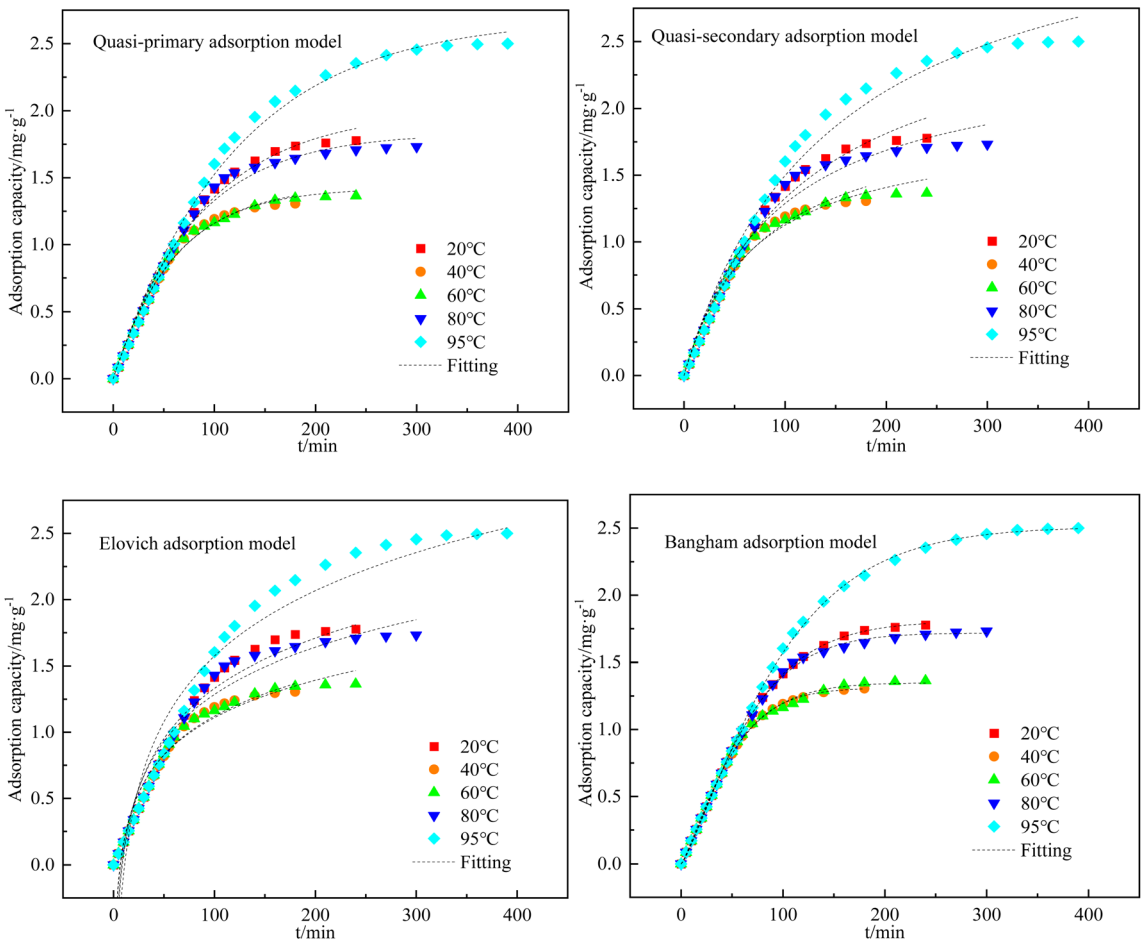

Fig. 7 Fitting curves of four kinetic equations for adsorption of H_2S by C-CS-B (3 : 5).

Table 3 Fitting results for kinetic equations

Kinetic equation	Parameters	Temperature				
		20 °C	40 °C	60 °C	80 °C	95 °C
Quasi-primary	q_e	1.99974	1.44155	1.42475	1.83317	2.69068
	k_1	0.01132	0.01630	0.01678	0.01291	0.00836
	R^2	0.99230	0.98985	0.99164	0.98860	0.99356
Quasi-secondary	q_e	2.85648	2.01711	1.88004	2.44068	3.69499
	k_2	0.00304	0.00644	0.00793	0.00458	0.00184
	R^2	0.98487	0.98061	0.98008	0.97486	0.98545
Elovich	α	0.20958	0.34527	0.37204	0.23987	0.12785
	β	1.83150	2.38407	2.45062	1.95160	1.40386
	R^2	0.94178	0.95486	0.96044	0.94543	0.94003
Bangham	q_e	1.80602	1.31016	1.34950	1.71820	2.50985
	n	1.25596	1.30355	1.22441	1.29637	1.22513
	k	0.00468	0.00599	0.00773	0.00430	0.00349
	R^2	0.99965	0.99924	0.99763	0.99886	0.99945

3.3. H_2S adsorption isotherms and kinetic

The H_2S adsorption equilibrium curves over C-CS-B (3 : 5) were drawn based on the points where the exit concentrations were 99% of the entrance concentrations ($C/C_0 = 99\%$) of 140, 280, 421, 561, 701, and 841 mg m^{-3} at different temperatures according to eqn (1) calculation of adsorption capacities.[19,20] The adsorption isotherms of H_2S on C-CS-B (3 : 5) were measured, and the results are shown in Fig. 6. The experimental data were analyzed following the isotherm models of Langmuir, Freundlich, and Temkin, and the parameters are listed in Table 2. Comparison of the correlation coefficients in Table 2 shows that the data were best-fitted by the Freundlich equation, implying that H_2S sorption is a surface sorption process.[21]

The Langmuir model is described by eqn (2):

$$\theta = q/q_m = bc/(1 + bc) \quad (2)$$

The fitted form of Langmuir model is described by eqn (3):

$$q = q_m bc/(1+bc) \quad (3)$$

where θ is the surface coverage; c is the equilibrium concentration (mg g^{-1}); q is the equilibrium adsorptive capacity (mg g^{-1}); q_m is the maximum adsorption capacity (mg g^{-1}); b is the Langmuir parameter.

The Freundlich model is described by eqn (4):

$$\theta = q/q_m = kc^n \quad (4)$$

The fitted form of Freundlich model is shown by eqn (5):

$$q = q_m kc^n \quad (5)$$

where n is the Freundlich parameter, and the other variable meanings are the same as those in eqn (2) and (3).

The Temkin model is described by eqn (6):

$$\theta = q/q_m = \ln a_0 c/f \quad (6)$$

where $(\ln a_0)/f = a$, $1/f = b$, and a and b are the curve parameters. The fitted form of Temkin model is described by eqn (7):

$$\theta = a + b \ln c \quad (7)$$

Where f and a_0 are the Temkin parameters, and the other variables meanings are the same as those in eqn (2) and (3).

The adsorption capacity of H_2S on C-CS-B (3 : 5) at different adsorption temperatures was calculated by eqn (1). The quasi-primary adsorption model, quasi-secondary adsorption model, Elovich adsorption model, and Bangham adsorption model were used to fit the data and determine the adsorption kinetic model most applicable to this experiment. The fitting results are shown in Fig. 7, and the calculated fitting parameters for each kinetic model are shown in Table 3. The results showed that the

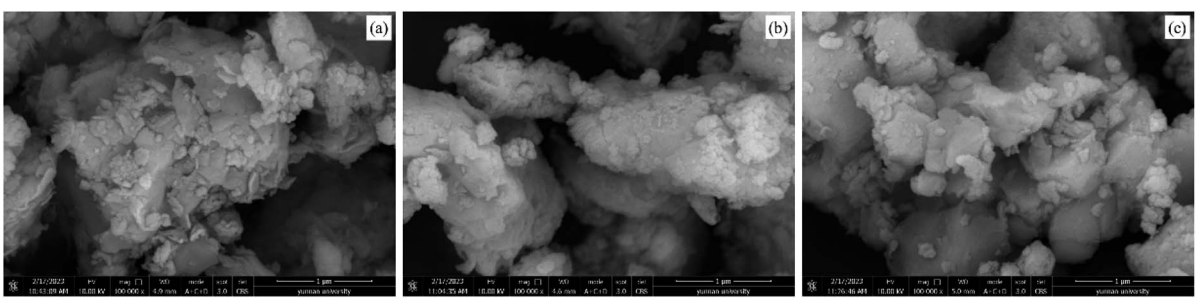

Fig. 8 SEM images of the surfaces of CK-B (a), C-CS-B (5 : 3) (b), and C-CS-B (5 : 3)-H_2S (c).

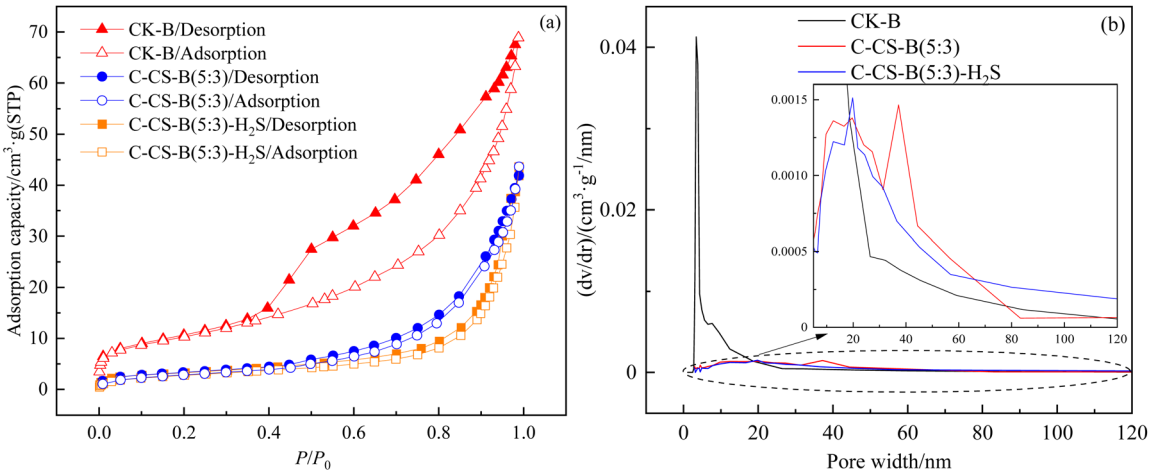

Fig. 9 N_2 adsorption/desorption isotherms (a) and pore size distribution curves (b) for CK-B, C-CS-B (5 : 3) and C-CS-B (5 : 3)-H_2S.

Table 4 Pore structure properties of different samples

Samples	BET surface area (m^2 g^{-1})	Total pore volume (cm^3 g^{-1})	Average pore size (nm)	Micropore volume (cm^3 g^{-1})
CK-B	38	0.107	0.11	0.015
C-CS-B (5 : 3)	12	0.065	0.22	0.004
C-CS-B (5 : 3)-H_2S	10	0.068	0.26	0.004

coefficient of determination was $R^2 > 0.99$ when fitting the data using the Bangham adsorption kinetic equation. Therefore, the Bangham adsorption kinetic model can describe the kinetic process of H_2S adsorption by C-CS-B (3 : 5).

The quasi-primary adsorption model differential equation is:

$$dq/dt = k_1(q_e - q_t) \quad (8)$$

After integrating eqn (8) from $t = 0$ to $t > 0$ ($q = 0$ to $q > 0$), the conversion equation is obtained as:

$$q_t = q_e - q_e e^{-k_1 t} \quad (9)$$

where q_t is the adsorption capacity at t time (mg g^{-1}); t is the adsorption time (min); q_e is the adsorption capacity at equilibrium (mg g^{-1}); k_1 is the quasi-primary adsorption rate constant.

The quasi-secondary adsorption model differential equation is:

$$dq/dt = k_2(q_e - q_t)^2 \quad (10)$$

After integrating eqn (10) from $t = 0$ to $t > 0$ ($q = 0$ to $q > 0$), the conversion equation was obtained as:

$$q_t = k_2 q_e^2 t/(1 + k_2 q_e t) \quad (11)$$

where k_2 is the quasi-secondary adsorption rate constant, other variable meanings were identical to those in eqn (8).

The Elovich adsorption model expression is:

$$q_t = (1/\beta)\ln(\alpha/\beta) + (1/\beta)\ln t \quad (12)$$

where α is the initial adsorption rate constant; β is the desorption rate constant, and other meanings were the same as those in eqn (8).

The Bangham adsorption model differential equation is:

$$dq/dt = k(q_e - q)/t^n \quad (13)$$

Integration of eqn (13) yields:

$$q_t = q_e - \frac{q_e}{e^{kt^n}} \quad (14)$$

where n and k are constants, and the other meanings were the same as those in eqn (8)

3.4. Adsorbent characterization

3.4.1. Effects on surface morphology. Fig. 8 reveals that the three samples showed a flocculent-like structure. The surface of sample CK-B (Fig. 8(a)) was extremely uneven and fractured because the grains of the primary mineral (montmorillonite) in bentonite were covered by particles of other minerals ($CaCO_3$, SiO_2, *etc.*). The surface of sample C-CS-B (5 : 3) was relatively flat, with small particles attached to the surface. This morphology might have been produced by the mixing of a large amount of carbide slag to fill the cracks on the bentonite surface, which reduced the specific surface area of the sample. The coverage of a large number of metal atoms made the adsorption of H_2S tend more towards chemisorption. According to Fig. 8(b) and (c), the surface morphology of sample C-CS-B (5 : 3) before and after H_2S adsorption was similar, showing that the adsorption of H_2S

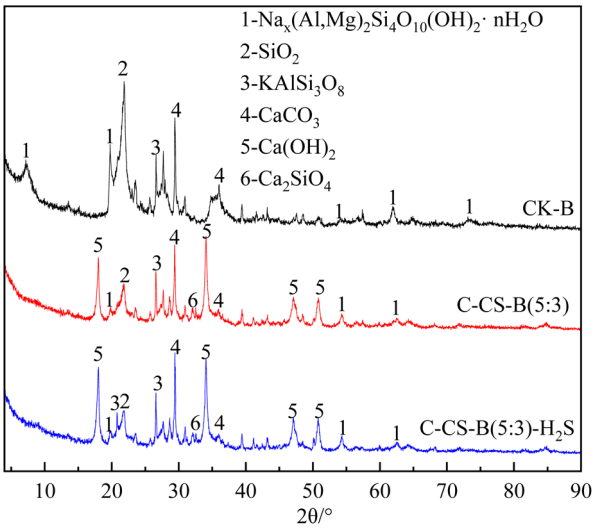

Fig. 10 XRD patterns of CK-B (a), C-CS-B (5 : 3) (b) and C-CS-B (5 : 3)-H_2S (c).

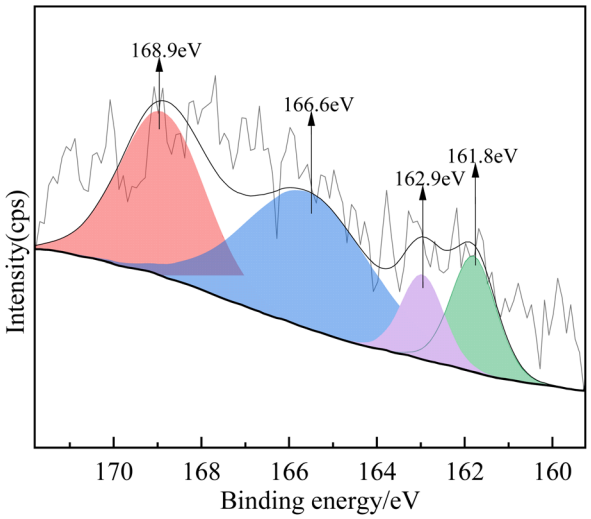

Fig. 12 XPS spectra (S 2p) of C-CS-B (5 : 3)-H_2S.

did not cause significant surface breakage or agglomeration. Sample C-CS-B (5 : 3) was defined as C-CS-B (5 : 3)-H_2S after the adsorption of H_2S.

3.4.2. N_2 adsorption–desorption and pore size distribution. As shown in Fig. 9(a), the adsorption capacity of the adsorbent modified by carbide slag was much lower than that of sample CK-B, which indicated that the pore volume and specific surface area of bentonite were reduced after mixing with carbide slag. In addition, most of the N_2 adsorption/desorption isotherms of porous adsorbent materials showed hysteresis loops due to capillary coalescence.[22] The isotherm shape of the CK-B sample formed an obvious H3-type hysteresis loop, which indicated that the pore structure of sample CK-B included flat slit-like pores, wedge-shaped structural pores, and fissure pores. Samples C-CS-B (5 : 3) and C-CS-B (5 : 3)-H_2S also formed an insignificant H3 hysteresis loop. Due to the complex pore structure of the materials, the hysteresis ring reflects the characteristics of the integrated pore structure. Based on the analysis of the bentonite, samples CK-B, C-CS-B (5 : 3), and C-CS-B (5 : 3)-H_2S were both laminar structures with flat slit-like pores and fissure pores.

The pore size distribution curves (Fig. 9(b)) of the samples were calculated by Barrett-Joiner-Halenda model.[23] The BET surface area, total pore volume, average pore size and micropore volume of the three samples are listed in Table 4. As seen from Fig. 9(b), the pore size distribution of sample CK-B was very different from that of other samples, and its pore size was mainly distributed in the mesoporous range of 2.7–18.4 nm. Comparisons between CK-B and C-CS-B (5 : 3) suggested that carbide slag modification blocked most pores, but it also expanded pores in the 19.6–83.4 nm size range. Combined with Fig. 9 and Table 4 and comparing C-CS-B (5 : 3) samples before and after adsorption, the specific surface area of C-CS-B (5 : 3)-

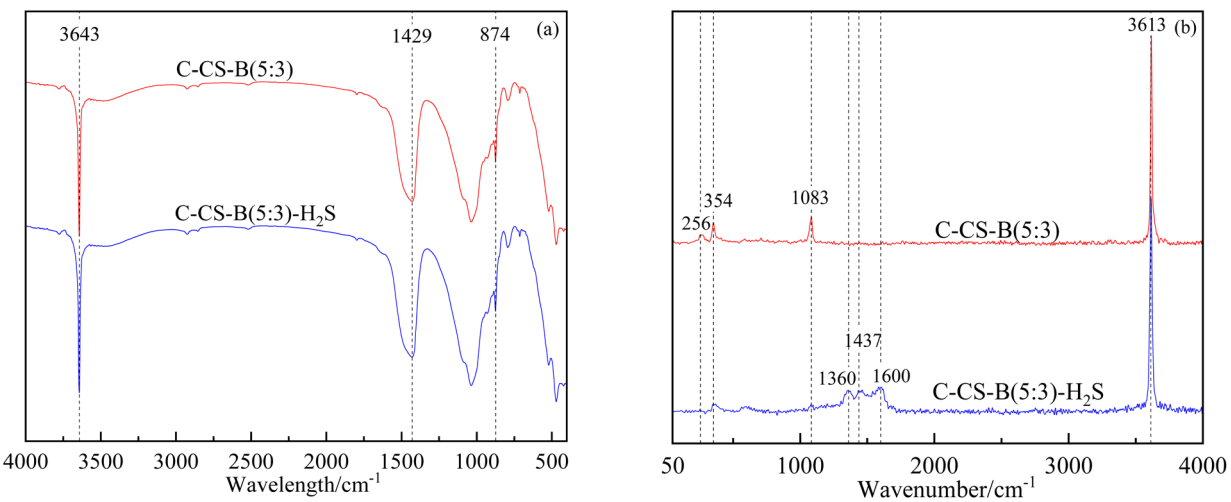

Fig. 11 FTIR spectrum (a) and Raman spectrum (b) of C-CS-B (5 : 3) and C-CS-B (5 : 3)-H_2S.

Table 5 XPS S 2p spectral data and their possible S states after H_2S adsorption

	Before adsorption	After adsorption	
S status	S 2p	Ca-S	SO_4^{2-}
Binding energy of S 2p (eV)	—	161.8	168.9
FWHM (eV)	—	2.03	3.06
Calculated S percentage (%)	0	0.27	0.42

H_2S decreased by 10%, and the total pore volume increased. H_2S underwent both pore filling (2.9–16.7 nm, 19.8–56.9 nm) and pore expansion (16.7–19.8 nm, 56.9–120 nm) on the adsorbent.

3.4.3. XRD analysis. XRD analysis (Fig. 10) showed that the composition of sample CK-B mainly included montmorillonite (Na_x (Al, Mg)$_2Si_4O_{10}(OH)_2 \cdot nH_2O$, JCPDS 12-0204), SiO_2 (JCPDS 89-3434), $KAlSi_3O_8$ (JCPDS 31-0966), and $CaCO_3$ (JCPDS 83-0578). After treatment with carbide slag, the crystal structure of the modified adsorbent C-CS-B (5 : 3) changed. A large amount of $Ca(OH)_2$ (JCPDS 78-0315) was loaded onto the adsorbent, and some SiO_2 in bentonite combined with CaO to form dicalcium silicate (Ca_2SiO_4, JCPDS 49-1673). In addition, the XRD peaks of the modified adsorbent C-CS-B (5 : 3) before and after the adsorption of H_2S did not change significantly. This indicated that the adsorption of H_2S did not affect the crystal structure of the adsorbent.

3.4.4. Spectral analysis. In the FTIR spectra of C-CS-B (5 : 3) and C-CS-B (5 : 3)-H_2S (Fig. 11(a)), two bands with almost complete overlap were observed. The band at 3643 cm^{-1} was assigned to the O–H stretching vibration of structural OH groups coordinated with the cation in the octahedral sheet.[24,25] Furthermore, a strong and broad peak at 1429 cm^{-1} and a weak and narrow peak at 874 cm^{-1} indicated the presence of $CaCO_3$.[26] These characteristic peaks all originated from $Ca(OH)_2$ and $CaCO_3$ in the carbide slag.

In the Raman spectra of samples C-CS-B (5 : 3) and C-CS-B (5 : 3)-H_2S (Fig. 11(b)), the peaks at 256 cm^{-1}, 354 cm^{-1}, and 3615 cm^{-1} represented O–H vibrations, which mainly originated from $Ca(OH)_2$.[27] The weakening of the O–H vibrational peak after the adsorption of H_2S by C-CS-B (5 : 3) indicated the involvement of hydroxyl groups in the adsorption process. The peaks of sample C-CS-B (5 : 3) at 1083 cm^{-1} and sample C-CS-B (5 : 3)-H_2S at 1437 cm^{-1} both represented telescopic vibration of CO_3^{2+} originating from the $CaCO_3$ component.[28] The change in the position of the spectral peaks before and after adsorption occurred because $CaCO_3$ was involved in the adsorption process and the crystalline form of $CaCO_3$ was changed. The Raman spectrum of the sample with adsorbed H_2S contained bands at 1360 cm^{-1} and 1600 cm^{-1}, which are characteristic of graphite.[29,30] The appearance of the carbon peaks indicates that a redox reaction involving the carbonaceous material occurred during adsorption.

3.4.5. XPS analysis. The valence states of atoms on the C-CS-B (5 : 3) were examined by XPS. Fig. 12 shows the XPS S2p spectrum after adsorption. The XPS fitting data of the S peaks, the possible S states, and their relative percentages are summarized in Table 5. As shown in Fig. 12, the fitted peaks at 161.8 eV and 162.9 eV were assigned to Ca-S $2p_{1/2}$ and Ca-S $2p_{3/2}$, while the peaks at 166.6 eV and 168.9 eV indicated the presence of $O–S^{2+}$ and SO_4^{2-}, respectively.[31–33] SO_4^{2-} was generated by oxidation, and the relative percentage of $CaSO_4$ (0.42%) was higher than that of CaS (0.27%) (Table 5), which indicates that $CaSO_4$ and CaS may be the species produced during H_2S adsorption.

3.5. Mechanism analysis of H_2S adsorption

Combining spectral (Fig. 11) and XPS (Fig. 12) characterization results, H_2S existed as CaS and sulfate on C-CS-B (3 : 5). As shown in Fig. 13, after the bentonite was modified by carbide slag, a large number of calcium atoms were introduced, and the surface of the sample was dominated by a large amount of $Ca(OH)_2$ and a small amount of $CaCO_3$. When H_2S diffused into the adsorbent, some H_2S reacted with $Ca(OH)_2$ to form CaS and $Ca(HS)_2$ *via* eqn (15) and (16). According to Sahu *et al.*,[34] the gas–solid reactions of H_2S on $CaCO_3$ were divided into two stages. First, $CaCO_3$ reacted with H_2S to form CaS, H_2O, and CO_2, then some of the products underwent redox reactions to form calcium sulfate dihydrate crystals ($CaSO_4 \cdot 2H_2O$) and singlet carbon. Eqn. (17) and (18) explain this process. Notably, when CO_2 and H_2O appeared in the system, $Ca(HS)_2$ was reconverted to $CaCO_3$ and H_2S by their combined action (eqn (19)). This process explains the appearance of a new $CaCO_3$ peak

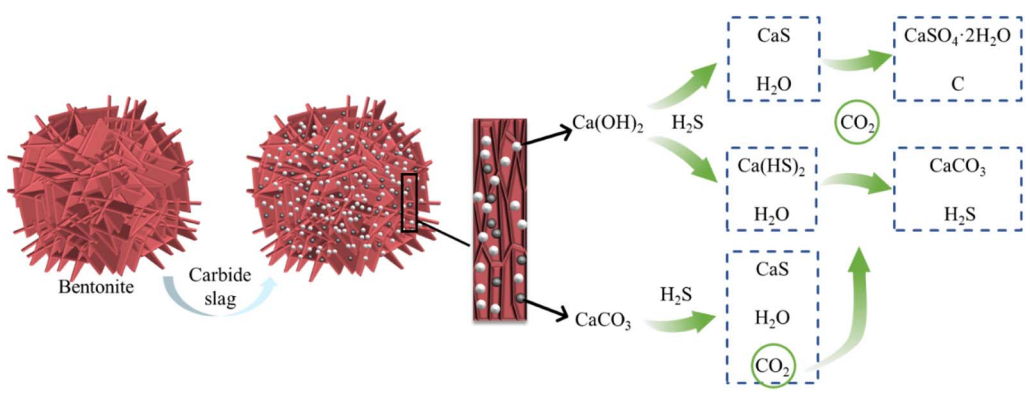

Fig. 13 The process of H_2S removal on C-CS-B (3 : 5) adsorbent.

(1437 cm^{-1}) in the Raman spectrum (Fig. 11). In addition, the hydrolysis of calcium sulfide at low temperatures made the adsorption of H_2S more suitable for high temperatures (eqn (20)).[35,36]

$$Ca(OH)_2 + H_2S \rightarrow CaS + 2H_2O \quad (15)$$

$$Ca(OH)_2 + 2H_2S \rightarrow Ca(HS)_2 + 2H_2O \quad (16)$$

$$CaCO_3 + H_2S \rightarrow CaS + H_2O + CO_2 \quad (17)$$

$$CaS + 2H_2O + 2CO_2 \rightarrow CaSO_4 \cdot 2H_2O + 2C \quad (18)$$

$$Ca(HS)_2 + H_2O + CO_2 \rightarrow CaCO_3 + 2H_2S \quad (19)$$

$$CaS + H_2O \rightarrow Ca(OH)_2 + H_2S \quad (20)$$

4. Conclusions

In this study, a H_2S adsorbent based on bentonite and carbide slag was prepared using bentonite, an abundant natural mineral, and carbide slag, an industrial waste. The preparation conditions of the adsorbent had a strong effect on the adsorption performance of H_2S. The mixture of carbide slag was proportional to the adsorption performance, and the best ratio was bentonite: carbide slag: water = 5 : 3: 5, and roasting at 450 °C for 2 h was the optimal preparation condition.

The adsorption capacity and breakthrough time of carbide slag-modified adsorbent were greatly improved compared with the single bentonite adsorbent. The adsorption temperature had a strong effect on the H_2S adsorption process, with higher temperatures favoring chemisorption. Under optimal conditions, the adsorption capacity of the carbide slag modified adsorbent for H_2S was 40 times higher than that of the blank bentonite-based adsorbent. The Freundlich isotherm model best described the adsorption of H_2S. The results of the computational fitting of the adsorption kinetics showed that the Bangham adsorption kinetic model beset described the kinetic process of H_2S adsorption by C-CS-B (5 : 3).

The adsorption of H_2S occurred *via* chemisorption, which occurred mainly in mesopores and macropores. An acid-base neutralization reaction, redox reaction, and hydrolysis reaction all occurred during adsorption. H_2S was removed in the form of CaS and sulfate.

Author contributions

Qi Jiang: Writing - original draft; Tianci Han and Yonglan Zong: writing - optimization and modification; Yongmei He and Youbo Su: supervision; Yonglin Wu and Bo Dian: writing - review and editing; Jilai Zhang: conceptualization; Tianguo Li: project administration; Ming Jiang: idea and funding acquisition.

Conflicts of interest

There are no conflicts to declare.

Acknowledgements

The authors gratefully acknowledge the National Natural Science Foundation of China (No 51768074) for the support.

References

1 H. Aljama, Z. Alaithan and A. Almofleh, *J. Phys. Chem. C*, 2023, **127**, 9022–9029, DOI: 10.1021/acs.jpcc.3c00903.
2 X. Zhou, L. Xu, S. Yang, S. Zhu, X. Chen, B. Dong, X. Bai, W. Xu, G. Lu and H. Song, *Sens. Actuators, B*, 2020, **309**, 127802, DOI: 10.1016/j.snb.2020.127802.
3 Q. Wang, Y. Chen, Y. Chen, D. Chen, X. Tian, J. Zhou, X. Li and Y. Wang, *Energy Fuels*, 2023, **37**, 1169–1179, DOI: 10.1021/acs.energyfuels.2c03067.
4 A. Ahmed, S. A. Onaizi and S. Elkatatny, *ACS Omega*, 2022, **7**, 28361–28368, DOI: 10.1021/acsomega.2c02890.
5 M. Askari, E. Salehi and A. Baluchi, *Chem. Eng. Res. Des.*, 2022, **188**, 545–554, DOI: 10.1016/j.cherd.2022.10.004.
6 A. T. Zoghi, M. Shokouhi, F. Naderi, M. Abbasghorbani, A. Fatehi, B. Pouladi and M. A. Adhami, *J. Solution Chem.*, 2022, **51**, 84–96, DOI: 10.1007/s10953-021-01131-1.
7 Q. Jiang, T. G. Li, Y. M. He, Y. L. Wu, J. L. Zhang and M. Jiang, *Environ. Chem. Lett.*, 2022, **20**, 1403–1419, DOI: 10.1007/s10311-021-01366-w.
8 S. Y. Jung, S. J. Lee, J. J. Park, S. C. Lee, H. K. Jun, T. J. Lee, C. K. Ryu and J. C. Kim, *Sep. Purif. Technol.*, 2008, **63**, 297–302, DOI: 10.1016/j.seppur.2008.05.013.
9 D. D. E. Koyuncu and S. Yasyerli, *Ind. Eng. Chem. Res.*, 2009, **48**, 5223–5229, DOI: 10.1021/ie8017059.
10 K. Yu, J. Xu, X. Jiang, C. Liu, W. McCall and J. Lu, *Chemosphere*, 2017, **184**, 884–891, DOI: 10.1016/j.chemosphere.2017.06.040.
11 X. Guo, Z. Wu, Z. Wang, F. Lin, P. Li and J. Liu, *ACS Omega*, 2023, **8**, 19455–19463, DOI: 10.1021/acsomega.3c00745.
12 W. Sun, J. Li, H. Li, B. Jin, Z. Li, T. Zhang and X. Zhu, *Chemosphere*, 2022, **296**, 133962, DOI: 10.1016/j.chemosphere.2022.133962.
13 K. V. Stepova, D. J. Maquarrie and I. M. Krip, *Appl. Clay Sci.*, 2009, **42**, 625–628, DOI: 10.1016/j.clay.2008.05.001.
14 D. Nguyen-Thanh and T. J. Bandosz, *Carbon*, 2005, **43**, 359–367, DOI: 10.1016/j.carbon.2004.09.023.
15 W. Tian, Z. Li, K. Zhang and Z. Ge, *RSC Adv.*, 2019, **9**, 19675–19679, DOI: 10.1039/c9ra02134e.
16 T. Wen, Y. Zhao, L. Chen, Y. Miao, Z. Zhang, S. Song and T. Zhang, *J. Cleaner Prod.*, 2023, **414**, 137650, DOI: 10.1016/j.jclepro.2023.137650.
17 Y. Li, W. Wang, X. Cheng, M. Su, X. Ma and X. Xie, *Fuel*, 2015, **142**, 21–27, DOI: 10.1016/j.fuel.2014.10.071.
18 X. Wang, Y. Ma, P. Ning, J. Qiu, X. Ren, Z. Li, W. Chen and W. Liu, *Adsorption*, 2014, **20**, 623–630, DOI: 10.1007/s10450-014-9607-y.
19 X. Wang, P. Ning, Y. Shi and M. Jiang, *J. Hazard. Mater.*, 2009, **171**, 588–593, DOI: 10.1016/j.jhazmat.2009.06.046.
20 M. Jiang, Z. Wang, P. Ning, S. Tian, X. Huang, Y. Bai, Y. Shi, X. Ren, W. Chen, Y. Qin, J. Zhou and R. Miao, *J. Taiwan Inst.*

Chem. Eng., 2014, **45**, 901–907, DOI: 10.1016/j.jtice.2013.08.008.
21 Q. Zhao, S. Tian, J. Zhang, S. Zhan, T. Sheng and P. Ning, *Can. J. Chem. Eng.*, 2015, **93**, 1247–1253, DOI: 10.1002/cjce.22208.
22 C. Sangwichien, G. L. Aranovich and M. D. Donohue, *Colloids Surf., A*, 2002, **206**, 313–320, DOI: 10.1016/S0927-7757(02)00048-1.
23 T. M. Oliver, K. Jugoslav, P. Aleksandar and D. Nikola, *Chem. Eng. Process.*, 2005, **44**, 1181–1187, DOI: 10.1016/s0140-6701(06)81163-x.
24 J. Madejová, *Vib. Spectrosc.*, 2003, **31**, 1–10, DOI: 10.1016/S0924-2031(02)00065-6.
25 M. Tanaka, A. Itadani, T. Abe, H. Taguchi and M. Nagao, *J. Colloid Interface Sci.*, 2007, **308**, 285–288, DOI: 10.1016/j.jcis.2006.12.002.
26 G. Wu, Y. Wang, S. Zhu and J. Wang, *Powder Technol.*, 2007, **172**, 82–88, DOI: 10.1016/j.powtec.2006.10.031.
27 Z. V. Pandanyi, *Solid State Commun.*, 1970, **8**, 541–543.
28 T. Schmid and P. Dariz, *J. Raman Spectrosc.*, 2015, **46**, 141–146, DOI: 10.1002/jrs.4622.
29 A. Manivannan, M. Chirila, N. C. Giles and M. S. Seehra, *Carbon*, 1999, **37**, 1741–1747, DOI: 10.1016/S0008-6223(99)00052-4.
30 I. Prasetyo and D. D. Do, *Carbon*, 1999, **37**, 1909–1918, DOI: 10.1016/S0008-6223(99)00065-2.
31 F. Zhu, X. Hu, L. Kong and X. Peng, *J. Hazard. Mater.*, 2022, **421**, 126745, DOI: 10.1016/j.jhazmat.2021.126745.
32 S. Zou, Y. Liao, S. Xiong, N. Huang, Y. Geng and S. Yang, *Environ. Sci. Technol.*, 2022, **51**, 3426–3434, DOI: 10.1021/acs.est.6b05765.
33 Z. Zhang, J. Wang, W. Li, M. Wang, W. Qiao, D. Long and L. Ling, *Carbon*, 2016, **96**, 608–615, DOI: 10.1016/j.carbon.2015.10.001.
34 R. C. Sahu, R. Patel and B. C. Ray, *Fuel Process. Technol.*, 2011, **92**, 1587–1592, DOI: 10.1016/j.fuproc.2011.04.002.
35 B. Sun, G. Yi, D. Chen, Y. Zhou and J. Cheng, *J. Mater. Chem.*, 2002, **12**, 1194–1198, DOI: 10.1039/b109352e.
36 M. Alla, A. Harrou, M. L. Elhafiany, D. Azerkane, M. El Ouahabi and E. K. Gharibi, *Phosphorus Sulfur*, 2002, **197**, 1026–1035, DOI: 10.1080/10426507.2022.2052881.